Modeling the effect of finite size gratings on scatterometry measurements

Elizabeth Kenyon,[*] Michael W. Cresswell,[*] Heather J. Patrick,[*†] and Thomas A. Germer[*]

[*]*National Institute of Standards and Technology, 100 Bureau Drive, Gaithersburg, MD 20899*
[†]*KT Consulting, Inc., 2545 10th Street, Suite A, Antioch, CA 94509*

ABSTRACT

The interpretation of scatterometry measurements generally assumes that the grating extends over an area large enough to intercept all the illumination provided by an incident beam. However, in practice, the gratings used in scatterometry are relatively small. Thus, the detected light also includes both that scattered by the grating as well as that from a region surrounding the grating because, generally, the incident beam illuminates both the grating and the surrounding region. To model the effects of such real structures, simulations of the effective reflectance were performed whereby the reflection from the grating was considered to be the sum of the diffraction by the grating and the diffraction of the surrounding region, taking into account the beam profile. To demonstrate the model, the illumination field was assumed to be Gaussian. Results are shown for a specific target design consisting of a 50 µm square measured by normal incidence reflectometry. Significant errors occur when the incident profile has wings that fall outside of the profile and when the scattered light is partially apertured.

Keywords: critical dimension, diffraction, gratings, metrology, process control, scatterometry, standards

1. INTRODUCTION

There has been a lot of recent interest in using the spectroscopic- and angle-resolved reflection properties of micro-gratings for critical dimension (CD) metrology in microfabrication applications.[1-3] Comparison of measured optical signatures with theoretically-determined signatures from model structures is used to deduce the dimensions and shape of the lines. Termed *scatterometry*, the technique has a number of advantages over competing techniques, such as atomic force microscopy (AFM) or scanning electron microscopy (SEM). For example, it can be configured as an in-line metrology, it is very sensitive, it statistically averages CD over a large number of lines, and it has high throughput. While scatterometry can be very precise, there are a number of issues that may detrimentally affect overall accuracy, such as accuracy of the optical properties used to simulate the signal, simplification of the profile, and line-edge and line-width roughness. In this manuscript, we consider the effects that finite grating size will have on scatterometry.

Scatterometry targets are typically square with side dimensions on the order of 50 µm to 100 µm. There is considerable industry pressure to reduce the dimensions of these targets, because real estate on product wafers is valuable. On the other hand, focusing onto the target is limited by the diffraction of the light. While a highly focused light source can be used, computation becomes significantly more intensive if the incident waves cannot be assumed to have a single incident angle. Inevitably, there is bleeding of the light into regions outside of the target, and reflected light from the surrounding regions contributes to the signal. Overfilling of the target will contribute to uncertainties in the measurement of target reflectance, and in turn, the extracted dimensions of lines.

In this manuscript, we make some preliminary estimates of the effects of finite target size. We assume that the target modulates the phase and amplitude of the reflected field differently than the surrounding region. We illuminate the target and surrounding region by applying a focused wave, and we treat the outgoing wave with Huygens-Fresnel diffraction theory. In Sec. 2, we develop the theory for diffraction by the target and the surrounding region, assuming that the target is square and illuminated with a Gaussian beam. In Sec. 3, we investigate the implications of the theory by considering illumination of a 50 µm square target with a Gaussian beam of 20 µm radius, using a variable size collection aperture and moving the sample around the center of the beam. We also consider the case of a spectroscopic measurement. We discuss the results in Sec. 4, and suggest possible tests for the effect of finite target size in a particular instrument. Finally, in Sec. 5, we make some conclusions.

This manuscript is a work of the U.S. Government and is not subject to copyright.
Metrology, Inspection, and Process Control for Microlithography XXII, Proc. SPIE **6922**, 69223P (2008).

Figure 1. Schematic of the problem considered and the approximation that is made in this paper. The square grating target is over-illuminated by a Gaussian beam (ellipse). The field scattered by the system is treated as the sum of the diffraction by the square target and that of the region outside the target.

2. THEORY

The target is assumed to consist of a single square region of dimensions $L \times L$, inside of which exists a periodic grating and outside of which exists a simple, potentially layered, medium. The target is illuminated at an angle θ_i with a focused beam, whose field E_{inc} in the plane of the sample is assumed to be a plane wave, modulated by an elliptically-elongated Gaussian profile,

$$E_{\text{inc}}(x,y) = \sqrt{\frac{2}{\pi w_0 \sec\theta_i}} \exp\left[-\frac{(x^2\cos^2\theta_i - y^2)}{w_0^{\,2}}\right] \exp\left(\mathrm{i}xk\sin\theta_i\right), \tag{1}$$

where the $1/\mathrm{e}^2$ beam radius is w_0, the magnitude of the propagation vector is $k = 2\pi/\lambda$, and λ is the wavelength. The z direction is along the surface normal, and the direction of the incident wave is assumed to be in the x-z plane. The wave in Eq. (1) is normalized to unit power. The principal approximation that will be made is illustrated in Fig. 1. That is, we will assume that the field diffracted by the target consists of a sum of the field diffracted by the inside and that diffracted by the outside. The intensity is then given by

$$I(k_x,k_y) = \left|S_{\text{inside}}(k_x,k_y)r_{\text{inside}} + S_{\text{outside}}(k_x,k_y)r_{\text{outside}}\right|^2, \tag{2}$$

where $S_{\text{inside}}(k_x,k_y)$ represents the scalar diffraction field for the Gaussian beam-illuminated target, $S_{\text{outside}}(k_x,k_y)$ represents the scalar diffraction field for the Gaussian-beam-blocked by the target, r_{inside} represents the complex reflectance coefficient of the target, and r_{outside} represents the complex reflectance coefficient of the region outside of the target. This approximation is valid if the target is large enough that the fields inside the target and those outside the target are not influenced by the edges of the target. The fields and intensities of the outgoing waves are treated as a function of the components, k_x and k_y, of the propagation vector onto the sample plane. In terms of the polar diffraction angle θ and azimuthal diffraction angle ϕ, these are given by

$$\begin{aligned} k_x &= k\sin\theta\cos\phi, \\ k_y &= k\sin\theta\sin\phi. \end{aligned} \tag{3}$$

According to the Huygens-Fresnel principle, the scalar diffraction of a Gaussian beam incident upon a square aperture is given by the truncated Fourier transform of Eq. (1),[4]

$$S_{\text{inside}}(k_x,k_y) = \frac{1}{2\pi}\int_{-L/2-x_0}^{L/2-x_0}\mathrm{d}x\int_{-L/2-y_0}^{L/2-y_0}\mathrm{d}y\; E_{\text{inc}}(x,y)\exp(-\mathrm{i}k_x x - \mathrm{i}k_y y), \tag{4}$$

which for the Gaussian beam profile given in Eq. (1) may be evaluated,

$$S_{\text{inside}}(k_x,k_y)=\frac{w_0}{4}\sqrt{\frac{\sec\theta_i}{2\pi}}e^{-\frac{1}{4}[(k_x-k\sin\theta_i)^2\sec^2\theta_i+k_y^2]w_0^2}\times$$
$$\left[\operatorname{erf}\left(\frac{L+\mathrm{i}(k_x-k\sin\theta_i)w_0^2\sec^2\theta_i-2x_0}{2w_0\sec\theta_i}\right)+\operatorname{erf}\left(\frac{L-\mathrm{i}(k_x-k\sin\theta_i)w_0^2\sec^2\theta_i+2x_0}{2w_0\sec\theta_i}\right)\right]\times \tag{5}$$
$$\left[\operatorname{erf}\left(\frac{L+\mathrm{i}k_yw_0^2-2y_0}{2w_0}\right)+\operatorname{erf}\left(\frac{L-\mathrm{i}k_yw_0^2+2y_0}{2w_0}\right)\right],$$

where $\operatorname{erf}(z)$ is the complex error function. The region of integration consists of the square target, which is offset in position by coordinates (x_0,y_0). Likewise, the scalar diffracted field from the region outside the target is given by

$$S_{\text{outside}}(k_x,k_y)=S_{\text{total}}(k_x,k_y)-S_{\text{inside}}(k_x,k_y)\,, \tag{6}$$

where

$$S_{\text{total}}(k_x,k_y)=\frac{1}{2\pi}\int_{-\infty}^{\infty}\mathrm{d}x\int_{-\infty}^{\infty}\mathrm{d}y\;E_{\text{inc}}(x,y)\exp(-\mathrm{i}k_xx-\mathrm{i}k_yy)=w_0\sqrt{\frac{\sec\theta_i}{2\pi}}\,\mathrm{e}^{-\frac{1}{4}[(k_x-k\sin\theta_i)^2\sec^2\theta_i+k_y^2]w_0^2}\,. \tag{7}$$

When we compute signals, we perform an integral over the intensity to yield a power,

$$P=\int\mathrm{d}k_x\mathrm{d}k_y\,\left|S_{\text{inside}}(k_x,k_y)r_{\text{inside}}+S_{\text{outside}}(k_x,k_y)r_{\text{outside}}\right|^2, \tag{8}$$

where the integral is over the region subtended by the detector aperture. We also compute the power one would measure from an infinitely conducting surface $(r_{\text{inside}}=r_{\text{outside}}=1)$,

$$P_{\text{ref}}=\int\mathrm{d}k_x\mathrm{d}k_y\,\left|S_{\text{total}}(k_x,k_y)\right|^2. \tag{9}$$

The measured *effective* reflectance of the sample is then

$$R=P/P_{\text{ref}}\,. \tag{10}$$

The complex coefficients r_{inside} and r_{outside} for reflection from the structures inside and outside the target, respectively, are dependent upon the polarization and were calculated using rigorous coupled wave (RCW) analysis.[5-7] The apertures considered in this study were all right circular cones having a half-angle α.

There are two limits that Eq. (8) can take. Either the fields add incoherently as intensities, so that

$$P=P_{\text{inside}}\left|r_{\text{inside}}\right|^2+P_{\text{outside}}\left|r_{\text{outside}}\right|^2, \tag{11}$$

where

$$P_{\text{inside}}=\int\mathrm{d}k_x\mathrm{d}k_y\,\left|S_{\text{inside}}(k_x,k_y)\right|^2 \tag{12}$$

and

$$P_{\text{outside}}=\int\mathrm{d}k_x\mathrm{d}k_y\,\left|S_{\text{outside}}(k_x,k_y)\right|^2, \tag{13}$$

or they add coherently as fields, so that

$$P=\left|\int\mathrm{d}k_x\mathrm{d}k_y\,\left[S_{\text{inside}}(k_x,k_y)r_{\text{inside}}+S_{\text{outside}}(k_x,k_y)r_{\text{outside}}\right]\right|^2. \tag{14}$$

The extent to which the actual behavior falls between these two limits can be expressed by a degree of coherence,

$$c = \left\langle S_{\text{inside}} S^*_{\text{outside}} \right\rangle \Big/ \left(\left\langle \left| S_{\text{inside}} \right|^2 \right\rangle \left\langle \left| S^*_{\text{outside}} \right|^2 \right\rangle \right)^{1/2}, \tag{15}$$

which takes the value $c = 0$ when the fields are incoherent, and $c = 1$ when they are coherent. The averages given in Eq. (15) are averages over the region subtended by the detector aperture.

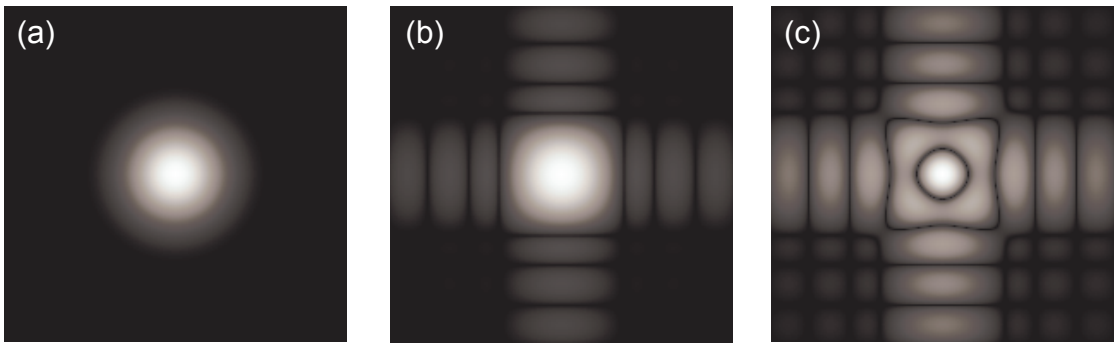

Figure 2. The diffraction pattern calculated for normally-incident Gaussian beam (a) without a target, S_{total}, (b) from inside of a square target, S_{inside}, and (c) from outside of a square target, S_{outside}. The target dimensions were 50 μm × 50 μm, the beam radius was 20 μm, and the horizontal and vertical scales are components of the diffracted propagation vector extending ±0.5 μm^{-1}. The gray scale corresponds to the square root of the absolute value of the field, chosen to enhance visualization of the pattern.

3. RESULTS

To illustrate the effects of finite target illumination, we choose a hypothetical square 50 μm × 50 μm target consisting of silicon lines of height 500 nm, width 40 nm, having vertical sides, and pitch 180 nm. These dimensions are close to those for a structure which we have fabricated.[8] The region surrounding the target consists of bare silicon, whose elevation is the same as that of the top of the grating lines. The outside elevation matters, because that determines the relative phase of the contributions inside and outside the target, if there is any coherence.

We first consider the coherence properties of the diffracted light to determine the regime an instrument is likely to operate in. For that, we consider a normally incident beam of wavelength 532 nm having a beam radius w_0 of 20 μm. Figure 2 shows the scalar diffraction pattern from the simply reflected beam (an infinite target), the finite target region, and the surrounding region. Because the target is not illuminated with a plane wave, the diffraction patterns from the target and the surrounding region are not complementary, but rather sum to the pattern with no diffraction screen. For that reason, they are not entirely coherent, and the degree of coherence depends upon how much of the diffracted pattern one collects. The diffraction patterns are in phase with one another at the center. An extra node (dark circle near the center) is observed in the pattern from the surrounding region. Outside of the node, the diffraction patterns will destructively interfere, reducing the coherence.

Figure 3 (left) shows the coherence parameters averaged over different size circular detectors. As expected, we find that as one increases the collection aperture, one collects more light. When α is about 0.75°, about 95% of the light diffracted by the target is collected. At this collection aperture, however, only about half of the light diffracted by the region outside the target is collected. This fact may suggest that it is best to operate with the collection aperture as small as possible, while still collecting most of the target-diffracted light. However, we find that such operation may be ill-advised for other reasons, which become apparent below.

Figure 3 also shows the degree of coherence averaged between the two diffraction patterns over the collection aperture. For a very small collection aperture, $c = 1$, and the fields from the diffraction sources interfere constructively. As the collection aperture increases, the degree of coherence drops. For a collection aperture with $\alpha = 0.75°$, the degree of coherence is about 11%. An effect of such coherence will be seen a little later in this paper.

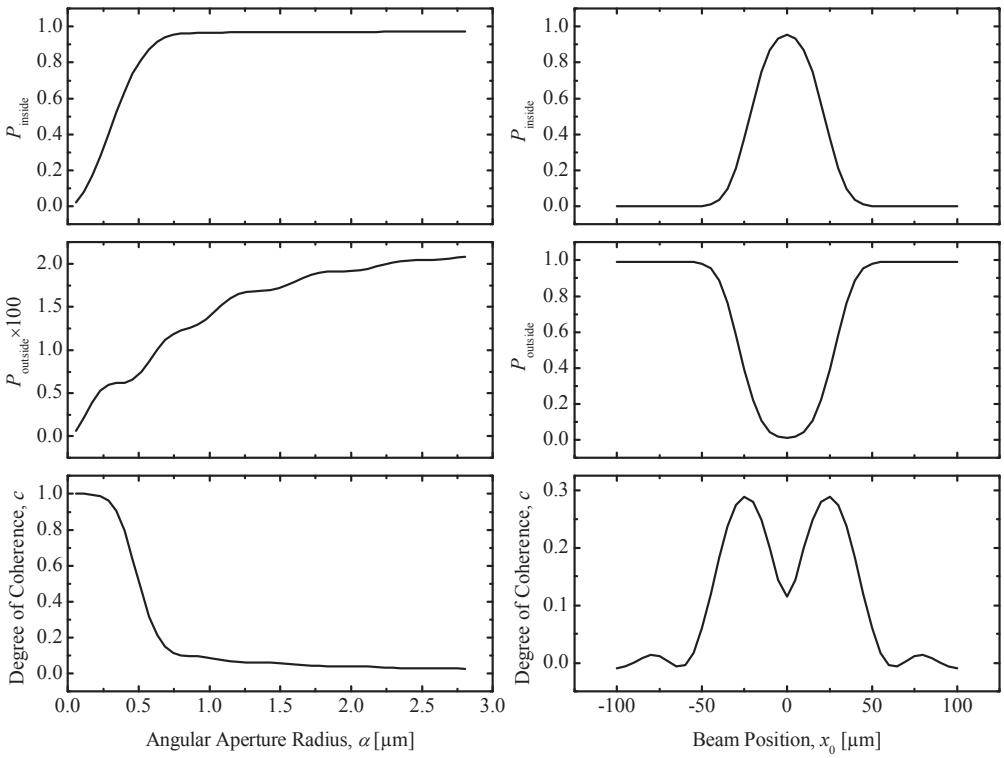

Figure 3. The fraction of light collected by a detector that comes from the target, P_{inside}, (top frames) and the region outside the target, $P_{outside}$, (middle frames) and the degree of coherence between them, c, (bottom frames). On the left, these quantities are calculated as a function of the collection half angle α when the incident beam is centered on the target. On the right, these quantities are calculated as a function of displacement of the beam on the target for a fixed $\alpha = 0.75°$. Other model parameters are described in the text.

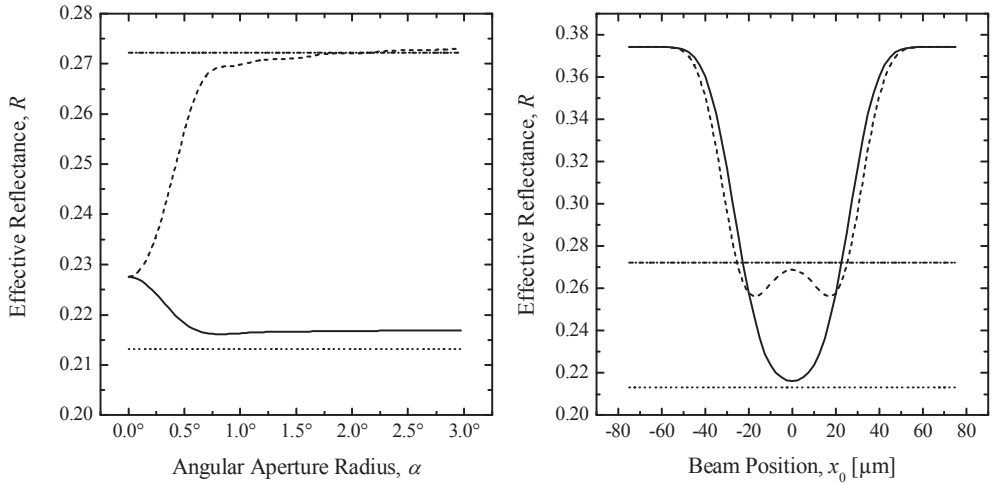

Figure 4. Effective s-polarized and p-polarized reflectance as functions of (left) the collection half-angle α when the incident beam is centered on the target and (right) the displacement of the beam on the target for a fixed $\alpha = 0.75°$. The curves are (solid) s-polarized signal for 50 μm target, and (dashed) p-polarized signal for 50 μm target. The horizontal lines represent the values for s-polarized signal for an infinite grating (dotted), and for p-polarized signal from an infinite grating (dash-dot).

Figure 3 (right) shows the coherence parameters for $\alpha = 0.75°$ as the target is translated through the beam. As expected, the diffracted power from the target collected by the aperture is at a maximum when the target is centered and falls off as the target is moved. Likewise, the light diffracted by the surrounding region increases as more light is incident upon that region. What is less intuitive is that the target dimensions, as judged by the width of the feature, appear different using the target and the surrounding regions, since the diffraction patterns differ. The coherence is largest when the two sources are equally illuminated.

Figure 4 shows simulations that include the effects of the finite target grating on a reflectance measurement. The results, as above, are for normal incidence, but show the s- and p-polarized effective reflectances. On Fig. 4 (left), the effective reflectances are shown as functions of aperture size for both a 50 μm target and an infinite target. For a small aperture, the results for the 50 μm target differ significantly from that predicted by an infinite one. Even at $\alpha = 0.75°$, there is still significant deviation between the finite-target and infinite-target predictions. (That the results are independent of polarization for $\alpha = 0$ is a coincidence.)

In Fig. 4 (right), we show the calculated effective reflectances as functions of the position of the beam on the target for $\alpha = 0.75°$. As seen in Fig. 4 (left), the effective reflectances differ from the nominal, infinite target parameters even at $x_0 = 0$. The light diffracted by the target and that diffracted by the surrounding material interfere differently depending upon where the beam is. An interesting observation can also be seen: the effective reflectance does not necessarily vary monotonically as one varies the position of the beam from centered. For the target considered, this was quite pronounced in the p-polarized signal, which exhibits a double lobed structure as the target is translated through the beam. We have observed this behavior in measurements of 60 μm square targets using a nearly Gaussian-limited beam of 15 μm spot size and a restricted collection aperture. The double-lobed structure disappears as the collection aperture is increased and the degree of coherence drops to zero.

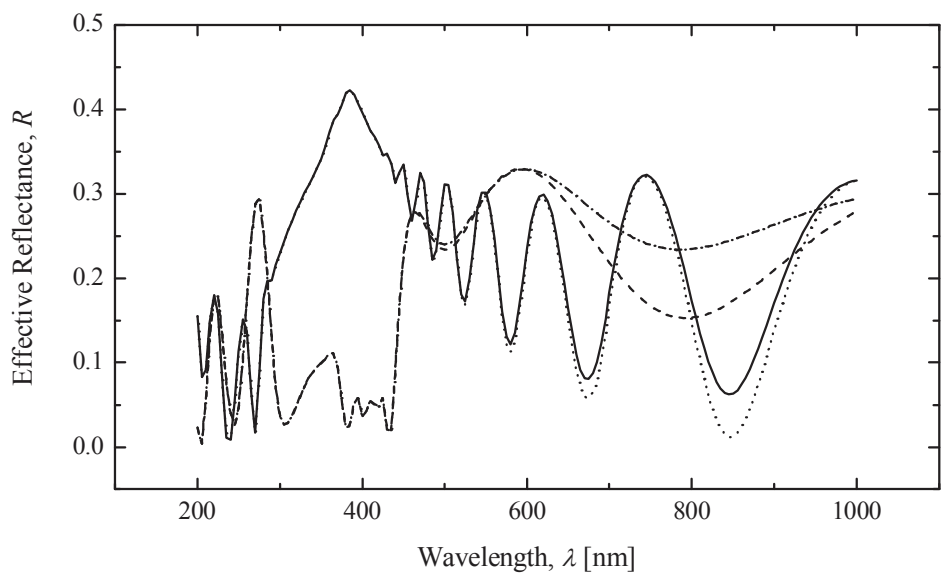

Figure 5. Predicted effective reflectance as a function of wavelength, assuming that the numerical aperture of the system is independent of wavelength. The curves are (solid) s-polarized signal for 50 μm target, (dashed) p-polarized signal for 50 μm target, (dotted) s-polarized signal for an infinite target, and (dash-dot) p-polarized signal for an infinite target.

We also performed a simulation of a spectroscopic scan. Here, we make the assumption that the f-number or numerical aperture of the illumination system remains constant. Under such conditions, the beam radius w_0 depends linearly upon the wavelength:

$$w_0(\lambda) = \lambda w_0(\lambda_1) / \lambda_1 . \tag{16}$$

We choose $w_0(532\text{ nm}) = 20\ \mu\text{m}$ and let the collection half-angle continue to be $\alpha = 0.75°$. Fig. 5 shows the effective reflectances as functions of wavelength for a 50 μm target and an infinite target. For wavelengths shorter than about 500 nm, there is little effect of the finite target, because the beam radius is very small. However, for longer wavelengths, there is progressively worse agreement.

4. DISCUSSION

The conditions used for the simulations described above were ideal and may not reflect a real operating environment. For example, it is rare that a diffraction-limited Gaussian beam is available. Performing the simulations on more realistic beams, however, adds significantly to the computational time, because the integrals in Eqs. (4) and (7) would need to be performed numerically. Furthermore, one would need to know not just the beam profile, but the phase profile as well. In reality, though, a realistic beam will have a profile with more energy in its wings than that for a single-mode Gaussian beam, so it is safe to say that the effects mentioned above are likely to be more pronounced.

The most interesting finding from the simulations is that there can be a net coherence between the light reflected by the target and that reflected by the surrounding region. Anytime fields add coherently, one sees interference effects, and those effects can be disproportionately greater than one might expect from intensity arguments alone. In particular, we observed some coherence when we apertured the reflected light and the incident beam profile had significant tails extending beyond the target.

Standardized tests may need to be developed to determine the extent that finite target size is having on a particular tool. One possibility is to have an array of targets having different sizes (L). Measurements performed on all of the targets could be made and compared. Above some target size, the signatures would remain constant, and one would know that target size would be the minimum target size that can be used. One particularly interesting target for such purposes would consist of bare silicon (with a native oxide), with the surrounding region having a thick dielectric coating (say, oxide or photoresist). In that case, one would not only know that the minimum acceptable target size has been reached, but also that the signature one obtains matches that expected from theory. The reflection properties of bare silicon, after all, are well known, and it is widely used as a standard target for ellipsometry and reflectance measurements Such a target would be easy to fabricate, since it does not require state-of-the-art fabrication techniques.

5. CONCLUSIONS

We have described a theoretical model for the reflection by a scatterometry target of finite size. We find that under some conditions, the measured reflectance is neither a coherent average nor an incoherent average of the reflectance over the illuminated part of the target. Effects were particularly pronounced when the incident beam had significant fields outside the target and the reflected light was apertured. A test is proposed for assessing the minimum target size that a tool can use.

ACKNOWLEDGEMENTS

Ms. Kenyon acknowledges the support of the Summer Undergraduate Research Fellowship program at NIST.

REFERENCES

1. S. A. Coulombe, B. K. Minhas, C. J. Raymond, S. Sohail, H. Naqvi, and J. R. McNeil, “Scatterometry measurement of sub-0.1 μm linewidth gratings,” J. Vac. Sci. Technol. B **16**, 80–87 (1998).
2. C. J. Raymond, M. R. Murnane, S. L. Prins, S. Sohail, H. Naqvi, J. R. McNeil, and J. W. Hosch, “Multiparameter grating metrology using optical scatterometry,” J. Vac. Sci. Technol. B **15**, 361–368 (1997).
3. C. J. Raymond, M. R. Murnane, S. S. H. Naqvi, and J. R. McNeil, “Metrology of subwavelength photoresist gratings using optical scatterometry,” J. Vac. Sci. Technol. B **13**, 1484–1495 (1995).
4. M. Born and E. Wolf, *Principles of Optics*, Chapter VIII (Pergamon, Oxford, 1980).

5. M. G. Moharam, E. B. Grann, D. A. Pommet, and T. K. Gaylord, "Formulation for stable and efficient implementation of the rigorous coupled-wave analysis of binary gratings," J. Opt. Soc. Am. A **12**, 1068–1076 (1995).

6. M. G. Moharam, D. A. Pommet, E. B. Grann, and T. K. Gaylord, "Stable implementation of the rigorous coupled-wave analysis for surface-relief gratings: enhanced transmittance matrix approach," J. Opt. Soc. Am. A **12**, 1077–1086 (1995).

7. P. Lalanne and G. M. Morris, "Highly improved convergence of the couple-wave method for TM polarization," J. Opt. Soc. Am. A **13**, 779–784 (1996).

8. H. J. Patrick, T. A. Germer, M. W. Cresswell, B. Li, H. Huang, and P. A. Ho, "Extraction of trench geometry and CD of nanoscale oriented silicon grating targets using angle-resolved scatterometry," to be published.